Proton Transfer in a Thr200His Mutant of Human Carbonic Anhydrase II

Deepa Bhatt,[1] Chingkuang Tu,[1] S. Zoë Fisher,[2] Jose A. Hernandez Prada,[2] Robert McKenna,[2]* and David N. Silverman[1,2]*

[1]*Department of Pharmacology and Therapeutics University of Florida, Gainesville, Florida*
[2]*Department of Biochemistry and Molecular Biology, College of Medicine, University of Florida, Gainesville, Florida*

ABSTRACT **Human carbonic anhydrase II (HCA II) has a histidine at position 64 (His64) that donates a proton to the zinc-bound hydroxide in catalysis of the dehydration of bicarbonate. To examine the effect of the histidine location on proton shuttling, His64 was replaced with Ala and Thr200 replaced with histidine (H64A-T200H HCAII), effectively relocating the proton shuttle residue ~ 2 Å closer to the zinc-bound hydroxide compared to wild type HCA II. The crystal structure of H64A-T200H HCA II at 1.8 Å resolution shows the side chain of His200 directly hydrogen-bonded with the zinc-bound solvent. Different proton transfer processes were observed at pH 6 and at pH 8 during the catalytic hydration-dehydration cycle, measured by mass spectrometry as the depletion of ^{18}O from $C^{18}O_2$ by H64A-T200H HCA II. The process at pH 6.0 is attributed to proton transfer between the side chain of His200 and the zinc-bound hydroxide, in analogy with proton transfer involving His64 in wild-type HCA II. At pH 8.0 it is attributed to proton transfer between bicarbonate and the zinc-bound hydroxide, as supported by the dependence of the rate of proton transfer on bicarbonate concentration and on solvent hydrogen isotope effects. This study establishes that a histidine directly hydrogen-bonded to the zinc-bound hydroxide, can adopt the correct distance geometry to support proton transfer. Proteins 2005;61:239–245.** © 2005 Wiley-Liss, Inc.

Key words: carbonic anhydrase; proton transfer; oxygen-18; histidine; isotope exchange

INTRODUCTION

Among the most efficient of the carbonic anhydrases in the α class is human carbonic anhydrase II (HCA II) which is widespread in many tissues and especially prominent in erythrocytes.[1,2] HCA II catalyzes the hydration/dehydration of CO_2 in two separate and distinct steps:[3,4]

$$CO_2 + EZnOH^- \leftrightarrow EZnHCO_3^- \overset{H_2O}{\leftrightarrow} EZnH_2O + HCO_3^- \quad (1)$$

$$EZnH_2O + B \leftrightarrow EZnOH^- + BH^+ \quad (2)$$

Here B is a proton acceptor, either part of the enzyme itself or an exogenous proton acceptor from solution. The rate-determining step in the maximal velocity of catalysis by HCA II is the proton transfer of Equation 2 in which a solvent accessible histidine, His64, at the rim of the active site cavity, acts as the proton acceptor in the hydration direction.[5,6] Replacement of His64 with Ala (H64A HCA II) results in a 10–50-fold decrease in the rate of catalysis compared with wild type.[6,7]

Several studies have estimated the function in catalysis of histidine residues at sites other than position 64 within the active-site cavity of carbonic anhydrase.[8–11] In general, it is concluded that His64 in HCA II is the most efficient site for proton transfer during catalysis. The side chain of His64 residue is located about 7.5 Å from the zinc, and extends into the active-site cavity with no predominant interactions with other residues. This site is too distant from the metal for direct proton transfer and therefore requires proton transfer through intervening water molecules. In this study, we investigated whether His200 in H64A-T200H HCA II could function as a proton shuttle. It has been previously shown that a mutant of HCA II in which Thr200 is replaced with Ser shows catalytic activity very close to that of wild type.[12] Previously, stopped-flow studies of the double mutant H64A-T200H HCA II showed it has about 5% of the activity of wild-type HCA II.[8] HCA I has a naturally occurring histidine residue at position 200 and has about 20% catalytic activity compared to HCA II, with a maximal turnover number in CO_2 hydration of 2×10^5 s^{-1}.[13] Replacement of Thr200 with histidine in HCA II (T200H HCAII) led to altered spectroscopic and catalytic properties such that the resulting mutant enzyme was similar to HCA I.[14] Additional amino-acid replacements at position 200 in HCA II were studied in CO_2 hydration and esterase activity.[15]

We have examined the proton transfer efficiency of His200 in H64A-T200H HCA II using an ^{18}O-exchange method and shown enhanced proton transfer is observed in the double mutant compared to the single mutant H64A

*Correspondence to: D.N. Silverman, Box 100267 Health Center, University of Florida, Gainesville, FL 32610-0267; E-mail: silvermn@college.med.ufl.edu; or R. McKenna, Box 100245 Health Center, University of Florida, Gainesville, FL 32610-0245; E-mail: rmckenna@ufl.edu

Received 27 January 2005; Revised 15 April 2005; Accepted 18 April 2005

Published online 16 August 2005 in Wiley InterScience (www.interscience.wiley.com). DOI: 10.1002/prot.20615

HCA II. Interestingly, this double mutant displayed two different proton transfer processes, one predominant at pH 6.0 and the other at pH 8.0. The proton transfer at pH 6.0 is consistent with His200 as donor and the zinc-bound hydroxide as acceptor, whereas as at pH 8.0 it is consistent with proton transfer from bicarbonate itself. Structural analysis using X-ray crystallography at 1.8 Å resolution indicated that the imidazole ring of His200 is within direct hydrogen-bonding distance of the zinc-bound solvent in the active site. Therefore we conclude that the imidazolium side chain of His200 can function as a proton shuttle. This is the closest position to the zinc in the active site of HCA II that a histidine has been placed and shown to transfer protons.

MATERIALS AND METHODS

Enzymes

The plasmid containing the gene encoding for the H64A and T200H mutations in HCA II was generously provided by Professor Sven Lindskog, Umeå University. This mutant of HCA II was expressed and purified by affinity chromatography methods, as described previously.[6,16] The enzyme concentration was determined from the molar absorbance of $5.5 \times 10^4\ M^{-1}cm^{-1}$at 280nm and by titration with the tight binding inhibitor ethoxzolamide. These two methods gave concentrations in excellent agreement.

Oxygen-18 Exchange

The rate of distribution of ^{18}O between CO_2 and water was measured using an Extrel EMX-200 mass spectrometer with a membrane inlet permeable to dissolved gases as described previously.[17] The rate of exchange of ^{18}O between ^{12}C -containing or ^{13}C-containing species of CO_2 at chemical equilibrium and rates of exchange of ^{18}O from species of CO_2 into water were measured. The ^{18}O exchange from bicarbonate to water, catalyzed by carbonic anhydrase, is shown in Equations 3 and 4:

$$HCOO^{18}O^- + EZnH_2O \leftrightarrow EZnHCOO^{18}O^- \leftrightarrow CO_2 + EZn^{18}OH^- + H_2O \quad (3)$$

$$EZn^{18}OH^- + BH^+ \leftrightarrow EZnH_2{}^{18}O + B \xrightarrow{H_2O} EZnH_2O + H_2{}^{18}O + B \quad (4)$$

Two kinetic parameters are determined by this method. The rate of interconversion of CO_2 and HCO_3^- at chemical equilibrium is R_1 as shown in Equation 5[18] where S in this work indicates total substrate, the sum of CO_2 and bicarbonate

$$R_l/[E] = k_{cat}^{ex}[S]/K_{eff}^{S} + [S] \quad (5)$$

The constant k_{cat}^{ex} describes the maximal rate of interconversion of CO_2 and bicarbonate at chemical equilibrium,[18] values which are not equivalent to the steady-state turnover number k_{cat}. However, the ratio k_{cat}^{ex}/K_{eff}^{S} is in principle and practice equal to the catalytic efficiency k_{cat}/K_m. The rate constant k_{cat}/K_m for the hydration of CO_2 for wild type HCA II can be adequately described by a single ionizable group;[13] however, in this study we found a second ionization affecting k_{cat}/K_m as expressed in the hydration direction:

$$k_{cat}/K_m = (k_{cat}/K_m)_{max1}/(1 + [H^+]/K_1) + (k_{cat}/K_m)_{max2}/(1 + [H^+]/K_2) \quad (6)$$

The proton transfer dependent rate constant for release of $H_2^{18}O$ from the enzyme into solvent is $R_{H2O}/[E]$, as described in Equation 4. For wild-type HCA II the bell-shaped pH profile for $R_{H2O}/[E]$ can be described in terms of the transfer of a proton from the imidazolium ion of His64 to a zinc-bound hydroxide.[17] However, in this study we observed that proton transfer in H64A-T200H HCA II showed two maxima, which we attribute to two independent proton transfer processes:

$$R_{H2O}/[E] = k_{B1}/[(1 + [H^+]/K_1)(1 + K_{B1}/[H^+])] + k_{B2}/[(1 + [H^+]/K_2)(1 + K_{B2}/[H^+])] \quad (7)$$

Here, K_1 and K_2 are the apparent or macroscopic, noninteracting ionization constants of the zinc-bound water in Equation 6, and K_{B1} and K_{B2} are the apparent or macroscopic, noninteracting ionization constants of the proton donors in catalysis. The values of k_B are rate constants for proton transfer under the condition of catalysis at chemical equilibrium.[17] Both Equations 6 and 7 assume that a sum of expressions for single proton transfer events is appropriate in cases of two independent proton transfer processes. Descriptions of these expressions for single proton transfers event are described previously.[10,17]

Proton Inventory

The solvent hydrogen isotope effect (SHIE) was determined at pH of 6.0 and 8.0. Appropriate concentrations of H_2O and D_2O were mixed together so that the deuterium concentration in the solvent mixture ranged from 0–99%. Sufficient Na_2SO_4 was added to maintain the ionic strength of the solvent at 0.2 M. All data for SHIE are reported using uncorrected pH meter readings. This allows a partial cancellation of two factors: pH meter correction for solvent D_2O (pD + 0.4) and the change in pK_a for almost all acids in the region of pK_a from 3–10 ($pK_{a\ (D2O)} - pK_{a(H2O)} \sim 0.5$).[19]

Crystallography

Crystals of H64A-T200H HCA II were obtained using the hanging drop method.[20] The crystallization drops were prepared by mixing 5 μL of protein (10.5 mg/mL concentration in 50 mM Tris-HCl, pH 7.8) with 5 μL of the precipitant solution (50 mM Tris-HCl, pH 7.8, 2.5–2.9 M ammonium sulfate) against 600 μL of the precipitant solution at 4°C. The pH of the crystals was determined by equilibrating them in appropriate buffers (50 mM Tris-HCl, pH 6.0 and 7.8; and 50 mM Caps, pH 9.3) in 3.0 M ammonium sulfate. Each crystal was equilibrated at the desired pH for at least 4 h at 4°C before commencement of data collection.

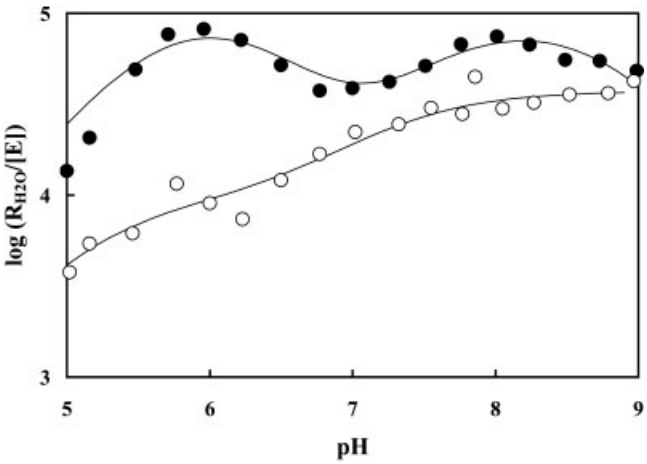

Fig. 1. The pH profile of the logarithm of R_{H2O}/[E] (s^{-1}) catalyzed by H64A HCA II (○), and H64A-T200H HCA II (●) at 25°C with solutions containing 25 mM of all species of CO_2 and sodium sulfate (ionic strength 0.2 M). No buffers were added. The solid line for H64A-T200H HCA II is a fit of Equation 7 to the data with the parameters given in Table I.

TABLE I. The Apparent Values of the pK_a for His200 and the Zn-bound Water Molecule, and the pH Independent Rate Constants (Maximal Values) for Proton Transfer in H64A, and H64A-T200H HCA II Determined From the Data of Figure 1

Enzyme	k_B[a] (μs^{-1})	$(pK_a)_{His200}$[b]	$(pK_a)_{Zn(H2O)}$[b]
wild-type HCA II[c]	0.8 ± 0.2	6.3 ± 0.3	7.2 ± 0.3
H64A HCA II	~0.05	—	—
H64A-T200H HCA II[d]	~0.3 − 0.5[e]	~5.9	~5.9
H64A-T200H HCA II[d]	~0.08[c]	7.7 ± 0.5	8.1 ± 0.5

[a]Values are from a least-squares fit of Equation 7 to the data of Figure 1.
[b]We have not specifically assigned these values of pK_a to His or to the zinc-bound water. That is, the data are equally well fit by interchanging these assignments. However, the values of $(pK_a)_{His200}$ and $(pK_a)_{Zn(H2O)}$ are so similar in each case that this specific assignment is not necessary.
[c]From Duda et al.[7]
[d]Two proton transfer process were observed for H64A-T200H HCA II.
[e]Values are uncertain due to small variation of R_{H2O} and limited range of pH.

X-ray-diffraction data sets were obtained with an R-AXIS IV++ image plate system with Osmic mirrors and a Rigaku HU-H3R Cu rotating anode operating at 50 kV and 100 mA. The detector to crystal distance was set to 100 mm. Each data set was collected at room temperature from single crystals mounted in quartz capillaries. The oscillation steps were 1° with a 3-min exposure per image. X-ray data indexing and processing were performed using DENZO and scaled and reduced with SCALEPACK software.[21]

The pH 6.0, 7.8, and 9.3 H64A-T200H HCA II structures were refined using the software package CNS, version 1.1[22] with interactive modeling using the graphics program O, version 7.[23] The wild type HCA II structure (Protein Data Bank accession number 2CBA[24]) was used to phase the data sets. To avoid phase bias of the model, residues Thr200 and His64 were mutated to Ala, and the zinc and water molecules were removed. After one cycle of rigid body, annealing, geometry-restrained positional, and temperature factor refinement, $(F_o - F_c)$ Fourier maps were generated. These density maps clearly showed the position of the zinc and mutated His200 residue, which were subsequently built into their respective maps. Model refinement continued with several iterative cycles of water molecule placement (using a 2.0σ density cut off) until convergence of the R_{cryst} and R_{free}.

These structures at pH 6.0, 7.8, and 9.3 have been deposited in the Protein Data Bank with the accession codes 1YO0, 1YO1, and 1YO2, respectively.

RESULTS

Catalysis by H64A-T200H HCA II

The rate constant R_{H2O}/[E] measures the proton-transfer dependent release of ^{18}O-labeled water from the enzyme (Equation 4). The double mutant H64A-T200H HCA II had a pH profile for R_{H2O}/[E] showing maxima near pH 6 and 8 (Fig. 1); each of these maxima is less than the single maximum for wild-type HCA II near $5 \times 10^5\ s^{-1}$ at pH 7.[7] However, each of these maxima is greater than that observed for the mutant lacking a proton shuttle residue H64A HCA II (Fig. 1). The pattern of two maxima observed in Figure 1 for R_{H2O}/[E] is consistent with two different proton transfer processes and can be fit by Equation 7 representing two independent proton transfers with constants given in Table I. However the narrow pH range of Figure 1 renders the derived kinetic parameters uncertain for H64A-T200H HCA II. Moreover, Equation 7 from which these parameters are obtained is based on the noninteracting ionization constants for the proton donor and acceptor. This approximation may lead to additional uncertainty since we have insufficient information to estimate the microscopic values of pK_a. However, we can point out that the apparent value of the pK_a for the zinc-bound water of H64A-T200H HCA II determined by a fit of the data of Figure 1 to Equation 7 is in agreement with the pH dependence of an independent parameter, that of k_{cat}/K_m for hydration of CO_2 (Fig. 4, Table I).

The substrate dependence of R_{H2O}/[E] at pH 8.5 is shown in Figure 2. At this pH, 98% of all species of CO_2 is bicarbonate; hence, this is viewed as an enhancement of R_{H2O}/[E] by bicarbonate. Figure 2(A) shows this enhancement is much smaller for H64A HCA II than for the double mutant. The substrate profile for H64A-T200H HCA II decreases at higher substrate concentrations [Fig. 2(A)], an unusual feature for carbonic anhydrase possibly indicating a substrate or product inhibition. At the very large concentrations of total substrate used in these experiments, it is possible that inhibitory binding sites for bicarbonate become important. Interestingly, the substrate profile of the mutant shows a much tighter binding of substrate in H64A-T200H than in H64A in which substrate binding is so weak we cannot measure it [Fig. 2(B)]. K^S_{eff} of Equation 5 for H64A-T200H is 130 ± 10 mM.

The rate constant R_{H2O}/[E] for catalysis by H64A-T200H HCA II was a linear function of n, the atom fraction of

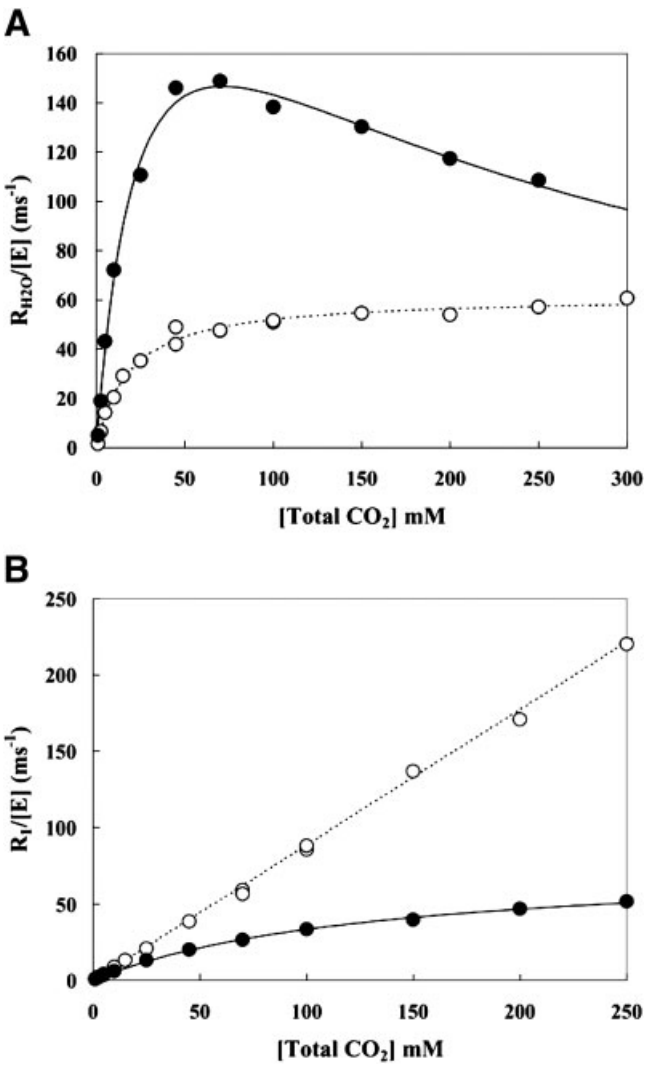

Fig. 2. **A**: The dependence of R_{H2O}/[E] on the concentration of all species of CO_2 at pH 8.5 and 25°C catalyzed by H64A HCA II (○), and H64A-T200H HCA II (●). No buffers were used and the total ionic strength of solution was maintained at a minimum of 0.2 M by addition of sodium sulfate. **B**: The dependence of R_1/[E] on the concentration of all species of CO_2. Conditions are the same as described for panel A.

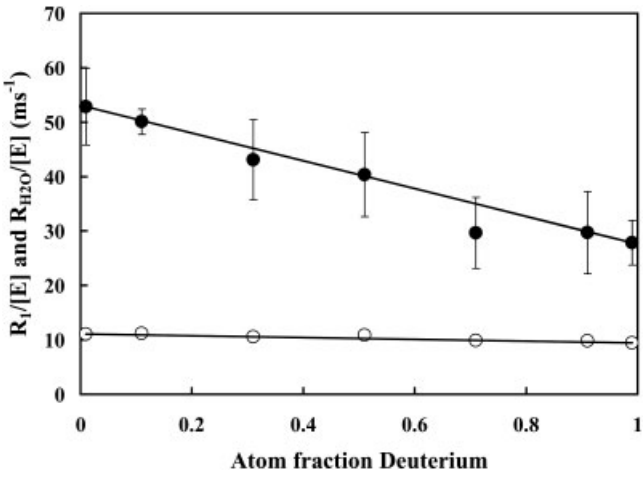

Fig. 3. Solvent hydrogen isotope effects (SHIE) on R_{H2O}/[E] (●) and R_1/[E] (○) in catalysis by H64A-H200T HCA II as a function of atom fraction of deuterium in solvent at pH 8.0. Experimental conditions were as described for Figure 1.

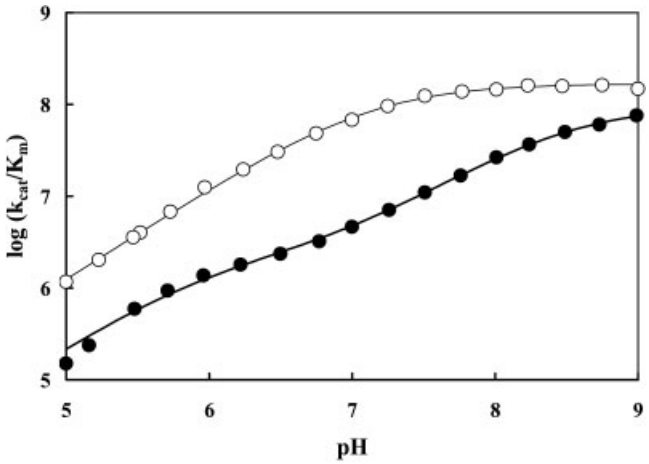

Fig. 4. The pH profile of the logarithm of k_{cat}/K_m ($M^{-1}s^{-1}$) for hydration of CO_2 catalyzed by H64A HCA II (○), and H64A-T200H HCA II (●). Experimental conditions were as described in Figure 1. For H64A-T200H HCA II the solid line is a fit to two ionizations (Equation 6) with pK_{a1} = 5.8 ± 0.4 and pK_{a2} = 8.0 ± 0.4. For H64A HCA II the data are fit to a single ionization with pK_a = 6.9 ± 0.1.

deuterium in solvent at pH 8.0 (Fig. 3). The solvent hydrogen isotope effect (SHIE) for R_{H2O}/[E] catalyzed by H64A-T200H HCA II under these conditions was 1.8 ± 0.2, consistent with a rate-contributing proton transfer step in catalysis. These data are an indication that one hydrogen changes the H/D fractionation factor going to the transition state of proton transfer.[19] A linear profile with SHIE of unity was found for R_1/[E] at pH 8.0 (Fig. 3), an observation showing that the interconversion of CO_2 and bicarbonate occurs without a proton transfer in rate-contributing steps. This is a conclusion reached some time ago using stopped-flow methods.[5] A similar experiment at pH 6.0 showed R_{H2O}/[E] was decidedly nonlinear and bulging down as a function of n (data not shown) with a SHIE of 1.7 ± 0.2. These results indicate that more than one hydrogen changes the fractionation factor upon going from the ground to transition state of the rate-contributing proton transfer of R_{H2O}/[E].[19] The SHIE for R_1/[E] was unity at pH 6.0.

The pH profile for k_{cat}/K_m for hydration of CO_2 catalyzed by H64A HCA II and measured by ^{18}O exchange (using Equation 6) could be described by a single ionization with pK 6.9 ± 0.1 (Fig. 4), a value very close to that of wild-type HCA II.[5,13] The pH profile for k_{cat}/K_m catalyzed by H64A-T200H HCA II was not described by a single ionization but an adequate fitting was obtained using the sum of two ionizations of pK_1 6.0 ± 0.5 and pK_2 8.5 ± 0.2 (Fig. 4). Although k_{cat}/K_m for this double mutant was lower by almost a 10-fold compared with wild type at and below pH 7.5, at pH 9 the catalytic efficiency as described by k_{cat}/K_m was comparable for H64A, for H64A-T200H HCA II (Fig. 4), and for wild-type HCA II.[5,13]

TABLE II. X-ray crystallographic data statistics for H64A-T200H HCA II at pH 9.3

Resolution shell (Å)	Number of reflections	Completeness (%)	R_{sym} [a]
500.0–4.34	1664	95.9	0.049
4.34–3.44	1628	97.2	0.059
3.44–3.01	1617	97.1	0.066
3.01–2.73	1599	96.1	0.075
2.73–2.54	1585	95.9	0.080
2.54–2.39	1564	95.0	0.083
2.39–2.27	1556	94.1	0.094
2.27–2.17	1537	93.8	0.101
2.17–2.09	1545	92.9	0.104
2.09–2.01	1529	92.8	0.119
2.01–1.95	1503	92.7	0.140
1.95–1.89	1490	90.1	0.159
1.89–1.85	1526	92.1	0.213
1.85–1.80	1408	87.3	0.282
500.0–1.80	21751	93.8	0.060

[a] $R_{sym} = \Sigma|I - \langle I\rangle|/\Sigma I$, where I is the intensity of a reflection and $\langle I\rangle$ is the average intensity.

TABLE III. X-Ray Crystallographic Refinement Statistics for H64A-T200H HCA II at pH 9.3

Space group	$P2_1$
Unit cell parameters (Å, °)	a = 42.6; b = 41.5; c = 72.7; β = 104.4
V_M ($Å^3 \times Da^{-1}$)	2.08
Calculated solvent content (%)	39
Resolution range (Å)	500.0–1.8 (1.85–1.80)[d]
Total observed reflections	52,409
Unique reflections/redundancy	21,751/2.4
I/I(σ)	11.3
Completeness (%)	93.8 (87.3)[d]
[a]R_{sym}	0.064 (0.282)[d]
[b]R_{cryst}/[c]R_{free}	0.168/0.201
Number of protein/solvent/ion atoms	3945/65/1
[c]RMSD bond lengths (Å)/angles (°)	0.005/1.36
Average B-factor protein main-/side-chain atoms ($Å^2$)	17.3/19.0
Average B-factor solvent/zinc ion ($Å^2$)	36.8/11.9
Ramachandran statistics (%)	
Most-favored/allowed/generously allowed	89.9/9.7/0.5

[a] $R_{sym} = \Sigma\,|I - \langle I\rangle|/\Sigma I$, where I is the intensity of a reflection and $\langle I\rangle$ is the average intensity.
[b] $R_{cryst} = \Sigma_{hkl}\,|F_o - KF_c|/\Sigma_{hkl}\,|F_o|$, R_{free} is calculated from 4.5% of data for cross-validation.
[c] RMSD = root mean square deviation.
[d] Data for the highest resolution shell are given in parentheses.

Crystal Structure of H64A-T200H HCA II

The structures for H64A-T200H HCA II at pH 6.0, 7.8, and 9.0 were all isomorphous to previously reported space group $P2_1$ wild type HCA II crystal structure (Protein Data Bank accession number 2CBA[24]) with unit cell dimensions a = 42.6, b = 41.5, c = 72.7 Å, and β = 104.4°. The structures for H64A-T200H HCA II at pH 6.0 and 7.8 showed anions (sulfate and/or chloride) bound in the active site and are not discussed here as they most likely represent crystallographic artifacts. The structure at pH 9.0 showed no bound ions and therefore depicted a noninhibited carbonic anhydrase. The H64A-T200H HCA II structure at pH 9.3 was obtained from 21,751 unique reflections (comp: 93.8%) to a resolution of 1.8 Å with an R_{sym} of 6.4% (Table II). The final refined structure had 65 well-ordered waters with an R_{cryst} of 16.8% and R_{free} of 20.1% (Table III).

The structure of H64A-T200H HCA II at pH 9.3 is similar to that of wild type HCA II with a root-mean-square deviation of Cα carbons of 0.2 Å. The coordination about the zinc including the zinc-bound hydroxide distance is comparable to wild type.[11] The imidazole ring of His200 is about 5 Å from the zinc and adjacent to the zinc-bound-hydroxide. The electron density for the side chain of His200 could be consistent with two conformations related by a rotation of the χ_2 torsion angle by 180° which cannot be differentiated at the resolution of these studies. In the conformer discussed in the next section, the nitrogen ND1 of His200 directly hydrogen bonds to the zinc-bound hydroxide at 3.1 Å (Fig. 5) with the χ_1 and the χ_2 torsion angles being 55° and 103° respectively. The alternate conformer would not form a hydrogen bond with the aqueous ligand of the zinc and is less consistent with, but not excluded by, kinetic data since it provides no apparent proton transfer pathway for catalysis.

DISCUSSION

In this study we examine proton transfer by His200 in H64A-T200H HCA II, the side chain of which is located closer to the zinc by about 2 Å than the histidine at residue 64, which is the proton shuttle in wild type HCA II. The basic question concerns the efficiency of proton transfer from the site of His200 to the zinc-bound hydroxide during catalysis of the hydration of CO_2. The data show that the mutant H64A-T200H HCA II had enhanced proton transfer in catalysis compared with H64A HCA II as measured by R_{H2O}/[E] (Fig. 1), a proton-transfer dependent rate constant for the release of $H_2^{18}O$ from the active site (Equation 4). This was not the case with the first stage of catalysis, the conversion of CO_2 into bicarbonate (Equation 1) as measured by k_{cat}/K_m (Figure 4).

Two well-separated maxima were observed in the pH profile of R_{H2O}/[E] catalyzed by H64A-T200H HCA II (Fig. 1) indicating two separate proton transfer processes. These data were fit by the sum of two bell-shaped curves (Equation 7) resulting in the constants of Table I. This is based on the interpretation of R_{H2O}/[E] described for wild-type HCA II in which a bell-shaped pH profile for R_{H2O}/[E] is observed consistent with proton transfer from His64 to the zinc-bound hydroxide.[7,17] This means that in the proton transfer process that predominates at low pH, the proton donor and acceptor both have conjugate acids with pK_a near 6 (Table I). We attribute this to the proton transfer from His200 to the zinc-bound hydroxide. The data of Figure 1 were adequately fit to a pK_a near 5.9 for both the imidazolium of His200 and for the zinc-bound water. These values are consistent with although somewhat

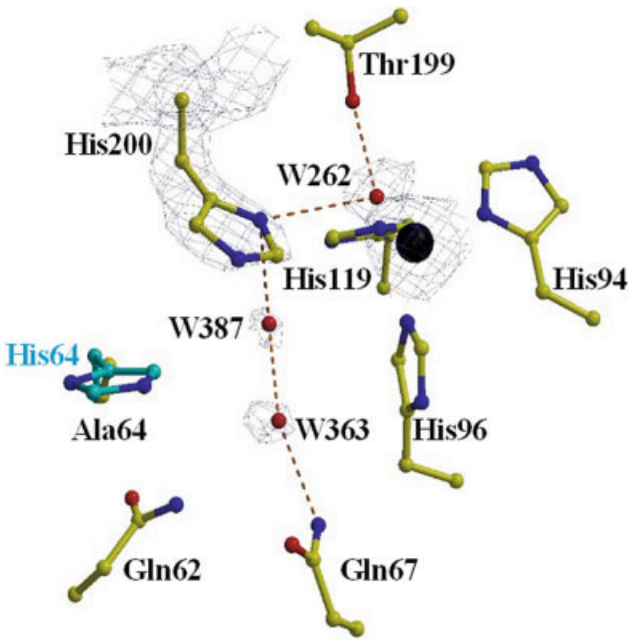

Fig. 5. The structure of the active site of H64A-T200H HCA II crystallized at pH 9.3. His94, His96, and His 119 and the zinc-bound solvent, W262, are direct ligands of the zinc. The dotted red lines indicate plausible hydrogen-bonds. The distance from W262 to ND1 His200 is 3.1 Å, from W262 to OG1 Thr199 is 2.7 Å, fromW387 to ND1 His200 is 3.1 Å, from W387 to W363 is 2.8 Å and from W363 to ND2 Gln67 is 2.8 Å. Electron density ($2F_o - F_c$) contoured at 1.5 σ (blue) is shown for His200, Zn^{2+}, W262, W363, and W387. Superimposed on Ala64 is the "in" orientation of the side chain of the proton shuttle residue His64 of wild-type HCA II.

lower than the pK_a of His64 and the zinc-bound water in wild-type HCA II which are both near 7.[13,25] However, depressed values of pK_a are frequently observed for histidine residues in the active-site cavity; a pK_a of 4.7 is observed for the imidazolium side chain of His64 in HCA I.[26] We note that the values of the pK_a for the zinc-bound water for H64A-T200H HCA II derived from the pH profile of k_{cat}/K_m, at 6.0 and 8.5 (Fig. 4), are very similar to those of Table I derived from $R_{H2O}/[E]$.

At high pH, the proton donor and acceptor in catalysis by H64A-T200H HCA II both have conjugate acids with pK_a near 8 (Table I). The properties of $R_{H2O}/[E]$ near pH 8 in Figures 1–3 are consistent with proton transfer from enzyme-bound HCO_3^- to metal-bound, ^{18}O-labeled hydroxide thus enhancing $R_{H2O}/[E]$ as demonstrated in Co(II)-substituted H64A HCA II by Tu et al.[27] The two values of pK_a near 8 correspond to those of HCO_3^- and the cobalt-bound water in the complex.[27] For both H64A-T200H and for Co(II)-substituted H64A HCA II the pH profile of $R_{H2O}/[E]$ is maximum at pH near 8, there is a strong dependence of $R_{H2O}/[E]$ on concentration of HCO_3^-, and there is a linear dependence of $R_{H2O}/[E]$ on the atom fraction of deuterium in solvent. Each of these properties was observed for H64A-T200H HCA II (Figures 1–3) and for ^{18}O exchange catalyzed by Co(II)-substituted H64A HCA II. In addition, a possibly related observation is that K_{eff}^S, an apparent substrate binding constant (Equation 5), indicates much tighter binding of substrate bicarbonate and/or CO_2 to H64A-T200H than to H64A HCA II [Fig. 2(B)]. Therefore, we interpret the maximum near pH 8 in Figure 1 as proton transfer from bound bicarbonate to the zinc-bound hydroxide. Again, we note that the values of the pK_a for the zinc-bound water for H64A-T200H HCA II derived from the pH profile of k_{cat}/K_m, near 6 and 8 (Fig. 4), are very similar to those of Table I derived from $R_{H2O}/[E]$.

It is significant that properties consistent with proton transfer from HCO_3^- in catalysis by carbonic anhydrase have been observed for two examples in which crystallography shows HCO_3^- bound to the zinc; Co (II)-substituted HCA II[24] and T200H HCA II.[28] In these cases, bicarbonate is observed to be a weak bidentate or pseudo-bidentate ligand of the metal, with the two oxygens of bicarbonate at about 2.2 and 2.5 Å from the metal.

A quantitative estimate of the efficiency of His200 in proton transfer is provided by the values of k_B shown in Table I, values obtained by a fit of Equation 7 to the data of Figure 1. These data at pH near 6 show that for H64A-T200H HCA II the maximal rate constant for proton transfer is about six- to 10-fold greater than the mutant H64A HCA II with no proton shuttle (Table I). There is likely a contribution of proton transfer from HCO_3^- involved at pH 6 as well since at this pH bicarbonate constitutes about 34% of all species of CO_2.

The crystal structure of H64A-T200H HCA II places the ND1 of the imidazole ring of His200 about 5.2 Å from the zinc and about 3.1 Å from the zinc-bound hydroxide (Fig. 5). This structure indicates a direct hydrogen bond between the imidazole ring of His200 and the zinc-bound solvent, suggesting that proton transfer during catalysis by H64A-T200H HCA II probably involves direct proton transfer with His200. It is interesting that the rate constant for proton transfer k_B near 0.3 – 0.5 μs^{-1} for H64A-T200H HCA II (Table I) is less than the values near 1 μs^{-1} for wild-type and H64A HCA II in which the proton donors are His64 and exogenous derivatives of imidazole and pyridine.[7,10] This shows that the position and conformation of the proton shuttle His200 are not optimal for the transfer of protons between the zinc-bound solvent molecule and bulk solution mediated by His200. Another factor to be considered is that His200, although close to the zinc-bound solvent, may be located too far from the surface of the enzyme to be efficient in proton transfer between the active site and bulk solution. Thus, we conclude that the imidazole side chain of His200 is active in proton transfer; however, it is not as efficient as His64 in HCA II.[5,6]

ACKNOWLEDGMENTS

We are grateful to Professor Sven Lindskog for providing a bacterial expression vector for H64A-T200H HCA II. We thank Lakshmanan Govindasamy for technical assistance. This work was supported by a grant from the NIH (GM 25154).

REFERENCES

1. Chegwidden WR, Carter ND, Edwards YH. The carbonic anhydrases new horizons. Basel: Birkauser Verlag; 2000.
2. Geers C, Gros G. Carbon dioxide transport and carbonic anhydrase in blood and muscle. Physiol Rev 2000;80:681–715.

3. Silverman DN, Lindskog S. The catalytic mechanism of carbonic anhydrase: implications of a rate-limiting protolysis of water. Acc Chem Res 1988;21:30–36.
4. Christianson DW, Fierke CA. Carbonic anhydrase: evolution of the zinc binding site by nature and by design. Acc Chem Res 1996;29:331–339.
5. Steiner H, Jonsson BH, Lindskog S. The catalytic mechanism of carbonic anhydrase. Hydrogen-isotope effects on the kinetic parameters of the human C isoenzyme. Eur J Biochem 1975;59:253–259.
6. Tu CK, Silverman DN, Forsman C, Jonsson BH, Lindskog S. Role of histidine 64 in the catalytic mechanism of human carbonic anhydrase II studied with a site-specific mutant. Biochemistry 1989;28:7913–7918.
7. Duda D, Tu CK, Qian M, Laipis P, Agbandje-McKenna M, Silverman DN, McKenna R. Structural and kinetic analysis of the chemical rescue of the proton transfer function of carbonic anhydrase II. Biochemistry 2001;40:1741–1748.
8. Liang Z, Jonsson BH, Lindskog S. Proton transfer in the catalytic mechanism of carbonic anhydrase. Effects of placing histidine residues at various positions in the active site of human isoenzyme II. Biochim Biophys Acta 1993;1203:142–146.
9. Briganti F, Mangani S, Orioli P, Scozzafava A, Vernaglione G, Supuran CT. Carbonic anhydrase activators: X-ray crystallographic and spectroscopic investigations for the interaction of isozymes I and II with histamine. Biochemistry 1997;36:10384–10392.
10. An H, Tu CK, Duda D, Montanez-Clemente I, Math K, Laipis PJ, McKenna R, Silverman DN. Chemical rescue in catalysis by human carbonic anhydrases II and III. Biochemistry 2002;41:3235–3242.
11. Fisher SZ, Hernandez J, Tu CK, Duda D, Yoshioka C, An H, Govindasamy L, Silverman DN, McKenna RM. Structural and kinetic characterization of active-site histidine in catalysis by carbonic anhydrase II. Biochemistry 2005;44:1097–1105.
12. Krebs JF, Fierke CA, Alexander RS, Christianson DW. Conformational mobility of His-64 in the Thr-200→Ser mutant of human carbonic anhydrase II. Biochemistry 1991;30:9153–9160.
13. Khalifah RG. The carbon dioxide hydration activity of carbonic anhydrase. J Biol Chem 1971;246:2561–2573.
14. Behravan G, Jonsson BH, Lindskog S. Fine tuning of the catalytic properties of carbonic anhydrase. Eur J Biochem 1990;190:351–357.
15. Behravan G, Jonasson P, Jonsson BH, Lindskog S. Structural and functional differences between carbonic anhydrase isoenzymes I and II as studied by site-directed mutagenesis. Eur J Biochem 1991;198:589–592.
16. Khalifah, RG, Strader DJ, Bryant SH, Gibson SM. Carbon-13 nuclear magnetic resonance probe of active-site ionizations in human carbonic anhydrase B. Biochemistry 1977;16:2241–2247.
17. Silverman DN. Carbonic anhydrase: Oxygen-18 exchange catalyzed by an enzyme with rate-contributing proton-transfer steps. Methods Enzymol 1982;87;732–752.
18. Simonsson I, Jonsson BH, Lindskog S. A ^{13}C nuclear-magnetic-resonance study of CO_2-HCO_3^- exchange catalyzed by human carbonic anhydrase C at chemical equilibrium. Eur J Biochem 1979;93:409–417.
19. Schowen, KB, Schowen, RL. Solvent isotope effects on enzyme systems. Methods Enzymol 1982;87:551–606.
20. McPherson A. Preparation and analysis of protein crystals. New York: Wiley; 1982.
21. Otwinoski Z, Minor W. Processing of X-ray diffraction data collected in oscillation mode Method Enzymol 1997;276:307–326.
22. Brunger AT, Adams PD, Core GM, Delano WL, Gross P, Grosse-Kunstleve RW, Jiang JS, Kuszewski J, Nilges N, Pannu NS, et al. Crystallography and NMR system: a new software suite for macromolecular structure determination. Acta Crystallogr 1998; D54:905–921.
23. Jones TA, Zou JY, Cowan SW, Kjeldgaard M. Improved methods for building protein models in electron density maps and the location of errors in these models. Acta Crystallogr 1991;47;110–119.
24. Håkansson K, Wehnert A. Structure of cobalt carbonic anhydrase complexed with bicarbonate. J Mol Biol 1992;228:1212–1218.
25. Campbell ID, Lindskog S., White, AI. Study of histidine residues of human carbonic anhydrase C using 270 MHz proton magnetic resonance. J. Mol. Biol. 1975;98:597–614.
26. Campbell ID, Lindskog S, White AI. Study of histidine residues of human carbonic anhydrase-B using 270 MHz proton magnetic resonance. J Mol Biol 1974;90:469–489.
27. Tu CK, Tripp BC, Ferry JG, Silverman DN. Bicarbonate as a proton donor in catalysis by Zn(II)- and Co(II)-containing carbonic anhydrases. J Am Chem Soc 2001;123:5861–5866.
28. Xue Y, Vidgren Y, Svensson LA, Liljas A, Lindskog S. Crystallographic analysis of Thr 200 → His human carbonic anhydrase II and its complex with the substrate HCO_3^-. Proteins 1993;15:80–87.